Multichannel quantum-defect analysis of the bound even-parity spectrum of neutral barium

M. Aymar and P. Camus

Laboratoire Aimé Cotton, Centre National de la Recherche Scientifique II, Bâtiment 505,
91405 Orsay Cedex, France

Extensive new data on the bound even-parity spectrum of neutral barium have been provided recently by two-step optogalvanic spectroscopy. Highly excited members of the Rydberg series $6sns\ ^3S_1$, $6snd\ ^3D_1, ^3D_3$, and $6sng$ as well as perturbing levels of these series belonging to $5dnd$ configurations have been observed. By means of multichannel quantum-defect theory (MQDT), we have performed the analysis of all available energy data relevant to the $J=1,3,4,5$ even-parity bound spectra of barium. The behavior of $6sns\ ^3S_1$, $6snd\ ^3D_1$, $^3D_3$ series perturbed by levels pertaining to the $5dns$ $(n=7,8)$ and $5dnd$ $(n=6,7)$ configurations is clearly interpreted. The MQDT analyses of $J=1$ and 3 spectra complementary to that previously performed on the $J=2$ spectrum offer the possibility of studying the anomalous fine structures of highly excited $6snd$ configurations. The MQDT analyses of $J=3-5$ spectra explain the observed energies of $6sng\ ^3G_{3,4,5}$ and $^1G_4$ Rydberg levels; the fine structures of the $6sng$ series are only partially resolved in the vicinity of $5d\,7d\ J=3$ to 5 perturbing levels. Since the $J=0$ and $J=2$ bound even-parity spectra of Ba have already been analyzed by MQDT, we have now a full MQDT description of the bound even-parity spectrum for J values ranging from 0 to 5.

I. INTRODUCTION

During the last ten years, many laser experiments have investigated the even-parity levels of neutral barium. Firstly, the highly excited bound levels of the $J=0$ and 2 spectra have been observed by Bradley et al.[1] and Rubbmark et al.[2] using absorption spectroscopy from excited levels populated by a dye laser; later, more extensive data concerning these spectra have been obtained by Aymar et al.[3] (to be referred to as AC) with the use of two-photon absorption spectroscopy and space-charge detection. All the experimental data[1-3] concern the principal Rydberg series $6sns\ ^1S_0$, $6snd\ ^1D_2, ^3D_2$ perturbed by levels of doubly excited configurations. These data have been successfully interpreted[3-5] by the multichannel quantum-defect theory (MQDT) introduced by Seaton[6] and elaborated by Lu, Fano, and co-workers.[7-10]

More recently, the spectroscopy of the even-parity spectrum of Ba has been enlarged through the observation of a great number of new levels by Armstrong et al,[11] Wynne and Herman,[12] and Camus et al.[13,14] Armstrong et al.[11] have observed members of $6sng\ ^1G_4$ series in a three-photon process via the $5d\,6p\ ^1F_3$ level. Wynne and Herman[12] have observed autoionized $5dnd$ and $5dns$ series with $J=0$, 1, and 2, converging on the $5d\ ^2D_{3/2}$ and

$5d\ ^2D_{5/2}$ ionization limits. A more extensive investigation of bound and autoionized even-parity spectra is being performed by Camus et al[13,14] using a two-step pulsed laser excitation combined with optogalvanic detection. Since the excitation process starts from the $5d\,6s\ ^3D_{1,2,3}$ and $^1D_2$ metastable levels populated in a discharge, the use of various $5d\,6p$ intermediate levels allows the observation of bound and autoionized levels with J values ranging from 0 to 5. Extensive new data concerning the bound spectrum are presented in Ref. 14 (to be referred to as CD); the analysis of the autoionizing region is still in progress.

The aim of this paper is to analyze the new spectroscopic data presented in CD on the bound levels with $J=1$, 2, 3, 4, and 5 by using MQDT. This work completes the analyses relevant to the $J=0$ and 2 spectra presented, respectively, in AC[3] and Aymar and Robaux[4] (AR). In fact, we expect that a good theoretical knowledge of the bound spectrum will help us in the analysis of the autoionized spectrum, which presents a more complicated scheme of interacting levels pertaining to the $5dnd$ configuration. The lowest $5dnd$ levels are bound, and the MQDT analysis involving interaction between $6snl$ and $5dnd$ channels should allow us to make contact with the autoionizing spectra.

The MQDT analyses presented below explain the behavior of the principal Rydberg series ($6sns\ ^3S_1$,

$6snd\ ^3D_{1,3}$ $6sng\ ^1G_4, ^3G_{3,4,5}$) when they are perturbed by the $5d\ 7s$, $5d\ 8s$, $5d\ 6d$, and $5d\ 7d$ levels. Moreover, the availability of data relevant to a large number of J values offers the possibility to analyze the fine structure of excited $6snl$ configurations and to examine the J dependence of the MQDT parameters.

II. BASIC FORMULAS OF MQDT

The MQDT analyses presented here closely follow AC[3] and AR,[4] and consequently, we will recall only some basic definitions. For an even-parity spectrum characterized by a given J value, the energies and wave functions of bound levels belonging to interacting Rydberg series converging to $6s$, $5d$, or $6p$ limits are expressed in terms of two sets of physically meaningful parameters. One set is formed with the elements of an orthogonal transformation matrix $U_{i\alpha}$ which connects the channel i of the dissociated system (electron and ion core) with the eigenchannel α of the same system in a close-coupling situation. The second set contains the eigenquantum defects μ_α of the close-coupling eigenchannels.

MQDT assigns to each energy level E as many effective quantum numbers ν_i as there are relevant series limits (N); each of them is defined by the equation

$$E = I_i - \frac{R}{\nu_i^2}, \tag{1}$$

where I_i is the ith series limit and R the mass corrected Rydberg constant. MQDT requires all the levels to lie on a surface $\mathscr{S}$ in the N-dimensional space of the ν_i, the analytical expression of which depends on μ_α and $U_{i\alpha}$. The $N-1$ independent relations

$$I_i - R/\nu_i^2 = I_j - R/\nu_j^2, \quad i \neq j$$

deduced from (1) determine a curve $\mathscr{L}$ in the same space. The theoretical positions of bound levels are given by the intersection of the curve $\mathscr{L}$ and the surface $\mathscr{S}$. The optimal MQDT parameters corresponding to a given J value are determined by comparison of experimental and theoretical energies.[15] The fitting has been carried out with Lu-Fano plots which present a graph of ν_i vs ν_j for various pairs of effective quantum numbers.

As in AC[3] and AR[4] we introduce a linear energy dependence of the eigenquantum defect as follows:

$$\mu_\alpha = \mu_\alpha^0 + \epsilon \mu_\alpha^1 \quad \text{with} \quad \epsilon = 1/\nu_{6s}^2. \tag{2}$$

We also follow AC[3] and AR[4] in factorizing the $U_{i\alpha}$ matrix, so that

$$U_{i\alpha} = \sum_{\bar{\alpha}} U_{i\bar{\alpha}} V_{\bar{\alpha}\alpha}. \tag{3}$$

The dissociated channels i are described in jj coupling, the intermediate $\bar{\alpha}$ channels are exactly LS coupled, and then the $U_{i\bar{\alpha}}$ are the elements of the well-known jj-LS transformation matrix. The $V_{\bar{\alpha}\alpha}$ matrix elements are expressed in terms of generalized Euler angles as described in Ref. 9.

III. ANALYSIS OF THE $J = 1$ AND $J = 3$ SPECTRA

The $J = 1$ bound spectrum is formed by two principal Rydberg series $6sns\ ^3S_1$ and $6snd\ ^3D_1$ and levels belonging to doubly excited configurations: $5dns\ ^3D_1$ ($n = 7,8$), $5dnd\ ^3D_1$, $^3S_1$, $^1P_1$, and $^3P_1$ ($n = 6,7$), and $6p^2\ ^3P_1$. The two $6snd\ ^3D_3$, and $6sng\ ^3G_3$ principal Rydberg series are perturbed by the $5dns\ ^3D_3$ ($n = 7,8$) and the $5dnd\ ^3G_3$, $^1F_3$, $^3D_3$, and $^3F_3$ ($n = 6,7$) levels. The new experimental data presented in CD[14] concern the highly excited $6sns$ and $6snd$ levels ($n > 11$), some $6sng$ levels, and the $5d\ 7d$ and $5d\ 8s$ levels. The energies of the lower levels are tabulated by Moore.[16] Data relevant to

TABLE I. $J = 1$ MQDT parameters.

| $\bar{\alpha}, \alpha, i$	1	2	3	4	5	6	7
$\bar{\alpha}$	$6ss\ ^3S_1$	$6sd\ ^3D_1$	$5dd\ ^3D_1$	$5dd\ ^3S_1$	$5dd\ ^1P_1$	$5dd\ ^3P_1$	$5ds\ ^3D_1$
i	$6s_{1/2}s_{1/2}$	$6s_{1/2}d_{3/2}$	$5d_{3/2}d_{3/2}$	$5d_{3/2}d_{5/2}$	$5d_{5/2}d_{5/2}$	$5d_{5/2}d_{3/2}$	$5d_{3/2}s_{1/2}$
μ_α^0	0.285	0.7715	0.805	0.713	0.779	0.573	0.1812
μ_α^1	0.4	1.0	0.85	1.65	0.67	0.22	0.44
	0.997	−0.004	0.030	−0.077	0	0	0
	0	0.884	−0.392	−0.197	−0.045	0	−0.155
	−0.037	0.292	0.721	−0.219	0.586	0	−0.051
$U_{i\alpha}$	−0.037	−0.225	−0.256	−0.580	0.212	0.707	0.040
	0.050	−0.046	−0.441	0.485	0.752	0	0.008
	0.037	0.225	0.256	0.580	−0.212	0.707	−0.040
	0	0.173	0	0	0	0	0.985
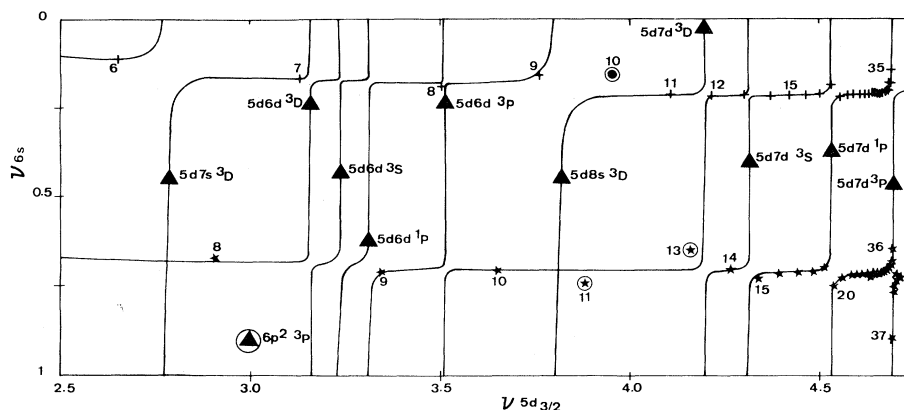
FIG. 1. Lu-Fano plot of the $J=1$ bound levels. Experimental points are $+$, $6snd\ ^3D_1$; $*$, $6sns\ ^3S_1$; ▲, perturbers. Note that the $6s\,10d\ ^3D_1$, the $6s\,11s\ ^3S_1$, the $6s\,13s\ ^3S_1$, and the $6p^2\ ^3P_1$ levels are ignored.

$6sng\ ^3G_3$ series will be analyzed in Sec. V, and only results relevant to the $6sns\ ^3S_1$ and $6snd\ ^3D_{1,3}$ perturbed series are presented here.

A. $J=1$ MQDT model

The $J=1$ bound spectrum is analyzed with a MQDT model involving seven channels and three limits. The labeling of the channels as well as the optimal parameters are compiled in Table I. The predicted Lu-Fano curve is plotted in Fig. 1.

The $6p^2\ ^3P_1$ level is excluded from the fit because there is no evidence that it perturbs either of the principal series. Some levels belonging to the principal series are also ignored. Firstly, the lowest levels ($6snd\ ^3D_1$ for $n=5$ and 6 and $6s\,7s\ ^3S_1$) are discarded because they are affected by core-polarization effects. Secondly, the high-lying $6snd\ ^3D_1$ ($36 \leq n \leq 38$) levels having a large uncertainty are also ignored. Finally, the $6s\,10d\ ^3D_1$ and $6s\,11s\ ^3S_1$

levels, found in Moore,[16] and the $6s\,13s\ ^3S_1$ level given in CD[14] are also excluded because their energy determinations appear to be questionable. The $6s\,10d\ ^3D_1$ and $6s\,11s\ ^3S_1$ levels are the highest $J=1$ even levels tabulated by Moore,[16] and they lie in an energy range where the compiled $6snd\ ^3D_2$ ($n=10,11$) levels have not been confirmed by the recent investigations of Refs. 1 and 2. The behavior of the $6s\,10d\ ^3D_1$ level cannot be interpreted by any perturbation as it clearly appears in Fig. 1. The interpretation of the $6s\,11s\ ^3S_1$ and $6s\,13s\ ^3S_1$ levels is rather difficult because the neighboring $6s\,12s\ ^3S_1$ is unknown. The anomalous small quantum defect of the $6s\,11s\ ^3S_1$ level located near the $5d\,8s\ ^3D_1$ level might be explained only by introducing a large interaction between the $6sns\ ^3S_1$ and $5dns\ ^3D_1$ channels. Since this mixing is expected to be vanishing in first approximation, we choose to neglect it. The interaction of the $6sns\ ^3S_1$ channel with the $5dnd$ channels are parametrized in terms of only one angle which allows one to generate the $V_{\bar{\alpha}\alpha}$ matrix defined

TABLE II. Parameters of the seven-channel MQDT model for the $J=3$ spectrum. The six-channel model (Sec. II) can be deduced by ignoring the last line and column.

| $\bar{a},\alpha,i$	1	2	3	4	5	6	7
$\bar{a}$	$6sd\ ^3D_3$	$5ds\ ^3D_3$	$5dd\ ^3G_3$	$5dd\ ^3F_3$	$5dd\ ^1F_3$	$5dd\ ^3D_3$	$6sg\ ^3G_3$
i	$6s_{1/2}d_{5/2}$	$5d_{5/2}s_{1/2}$	$5d_{3/2}d_{3/2}$	$5d_{5/2}d_{3/2}$	$5d_{3/2}d_{5/2}$	$5d_{5/2}d_{5/2}$	$6s_{1/2}g_{7/2}$
μ_α^0	0.76	0.1868	0.763	0.6576	0.785	0.826	0.0585
μ_α^1	0.66	0.46	1.18	0.4	1.36	0.86	-0.8
	0.918	-0.149	-0.102	0.089	-0.117	-0.321	-0.005
	0.139	0.989	-0.015	0.013	-0.018	-0.048	-0.001
	0.025	0	0.866	0.002	0.366	-0.337	0.043
$U_{i\alpha}$	0.040	0	0.349	0.705	-0.488	0.376	0.017
	-0.158	0	-0.339	0.704	0.503	-0.334	-0.017
	0.333	0	0.019	0	0.600	0.727	0.001
	0	0	-0.050	0	0	0	0.999
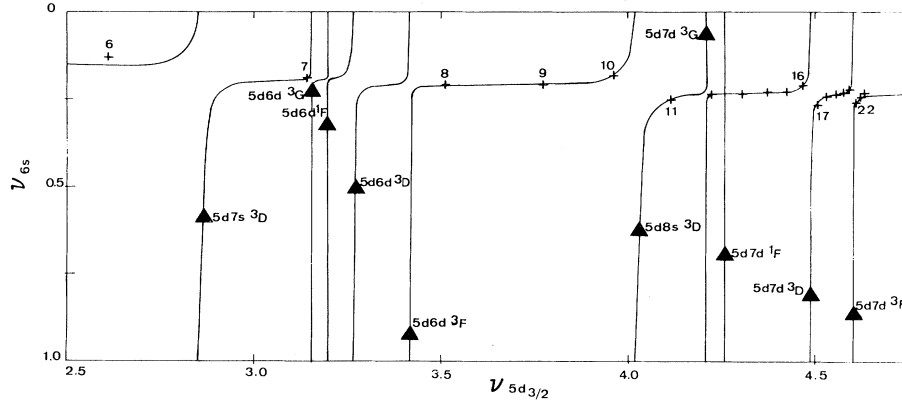
FIG. 2. Lu-Fano plot of the $J = 3$ bound levels. Experimental points are $+$, $6snd\ ^3D_3$ and ▲, $5dnl$.

in Eq. (3) by coupling the $6sns\ ^3S_1$ and $5dnd\ ^3S_1$ channels.

The Lu-Fano curve (Fig. 1) shows a reasonable agreement with the experimental data; the perturbation of high-lying levels are very well reproduced. However, further measurements in the intermediate energy range are needed for improving the fit.

B. $J = 3$ MQDT model

The $J = 3$ bound spectrum is analyzed with a MQDT model involving six channels and three limits. The labeling of the channels and the optimal parameters are compiled in Table II. All $J = 3$ levels except the two lowest $6snd\ ^3D_3$ ($n = 5, 6$) levels, which are excluded from the fit, are successfully interpreted as can be seen from the Lu-Fano curve plotted in Fig. 2.

IV. FINE STRUCTURES
OF $6snd$ CONFIGURATIONS

The fine structures of the $6snd$ triplets can be analyzed from the MQDT analyses presented above or in AR.[4] The fine structure of the "unperturbed" $6snd$ triplets (i.e., neglecting the perturbations affecting the $6snd\ ^3D$ series) can be studied from the eigenquantum defects $\mu_{3_{D_1}}$, $\mu_{3_{D_2}}$, and $\mu_{3_{D_3}}$. One must notice that, far from any perturbations, the $6snd\ ^3D_2$ and $^1D_2$ series are well described in LS coupling.[4] Consequently, the unperturbed $6snd\ ^3D$ levels are expected to satisfy the Landé interval rule[17]; then the ξ_{nd} spin-orbit parameter of the outer nd electron can be deduced from differences between eigenquantum defect as shown on the following formula:

$$\xi_{nd} = \frac{2R}{n_*^3}(\mu_{3_{D_1}} - \mu_{3_{D_2}}),$$ (4a)

$$\xi_{nd} = \frac{4R}{3n_*^3}(\mu_{3_{D_2}} - \mu_{3_{D_3}}),$$ (4b)

$$\xi_{nd} = \frac{4}{5}\frac{R}{n_*^3}(\mu_{3_{D_1}} - \mu_{3_{D_3}}),$$ (4c)

where $n^* = \nu_{6s}$ is the average effective quantum number of $6snd\ ^3D$ levels.

The energy-dependent eigenquantum defect obtained for $J = 1, 2, 3$ are compiled in Table III. From μ_α^0 values we deduce the asymptotical value $\bar{\xi} = n^{*3} \times \xi_{nd}$ when $n \to \infty$. One can see that the Landé interval rule is well satisfied within the uncertainty of the μ_α^0 values. If the energy dependence of eigenquantum defects is taken into account, the Landé interval rule is less well satisfied due to large differences between μ_α^1 values; this point will be discussed later in Sec. VI. The ξ_{nd} values obtained from Eq. (4c) for $n = 20$ are also tabulated in Table III.

In Fig. 3 we have plotted part of the three theoret-

TABLE III. Fine structure of $6snd$ configurations: $6snd\ ^3D$ eigenquantum defect and ξ_{nd} spin-orbit parameter calculated from eigenquantum defect with the Landé rule.

	Eigenquantum defect	
	μ_α^0	μ_α^1
$^3D_1$	0.7715	1.0
$^3D_2$	0.7668	1.03
$^3D_3$	0.76	0.66

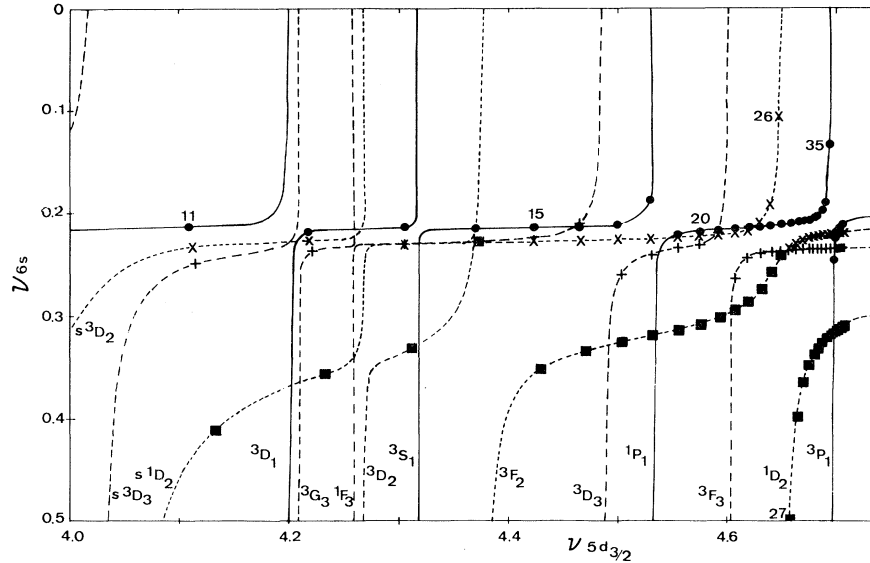| Spin-orbit parameter (cm^{-1})		
$\bar{\xi} = n^{*3}\xi_{nd}$ for $n \to \infty$		
1030	calculated from	$\mu_{3_{D_1}}^0 - \mu_{3_{D_2}}^0$
990	calculated from	$\mu_{3_{D_2}}^0 - \mu_{3_{D_3}}^0$
1010	calculated from	$\mu_{3_{D_1}}^0 - \mu_{3_{D_3}}^0$
ξ_{20d}		
0.20	calculated from	$\mu_{3_{D_1}}^0 - m_{3_{D_3}}^0$
0.22	calculated from	$\mu_{3_{D_1}} - \mu_{3_{D_3}}$

FIG. 3. Lu-Fano plot of the $6snd$ perturbed Rydberg series. Curves and predicted energies reported on the curves are calculated from MQDT models either compiled in the tables or developed in AR. The symbols are ——●——, $6snd$ $^3D_1$; ---X---, $6snd$ $^3D_2$; ---■---, $6snd$ $^1D_2$; and — — — + — — — — $6snd$ $^3D_3$. Perturbers are only noted by the vertical branches they cause in the curves; the symbols are s $^{2S+1}L_J$ for $5d\,8s$ levels and $^{2S+1}L_J$ for $5d\,7d$ perturbers.

ical Lu-Fano curves obtained here or in AR[4] for $J = 1,2,3$ spectra. One can see by following the point ($^3D_1$), cross ($^3D_2$), and plus ($^3D_3$) marks along the $6snd$ ^3D series that the triplet levels do not satisfy the Landé interval rules. This anomalous behavior is clearly related to the presence of $5dnl$ perturbers; some $6snd$ ^3D levels are strongly repelled by perturbers, and moreover, the $5d\,7d$ $^1D_2$ perturber induces a singlet-triplet mixing in the high-energy range. Although experimental points are not included in the figure for purposes of clarity, the predictions of MQDT concerning the relative position of the three members of the same triplet are generally in very good agreement with experimental data. In particular, the coincidences or quasicoincidences predicted for $n = 13-15$ or for $19 < n < 24$ confirm the experimental observations.

We recall that the previous identifications of the $J = 1$ and 3 levels in CD[14] were facilitated by the knowledge of $J = 2$ levels from AC.[3] Nevertheless, for high n values, the observed signals are difficult to identify because the experimental resolution is too low. Moreover, the uncertainty is of the same order of magnitude as the intervals between the components of the triplets, so the $6snd$ $^3D_3$ ($n > 24$) levels which were not identified are certainly unresolved from the $6snd$ $^3D_2$ levels.

V. ANALYSIS OF THE $6sng$ SERIES

In CD[14] a great number of levels has been identified as the $6sng$ levels with $8 \leq n \leq 39$. Owing to the very small values of both the spin-orbit coupling constant for an ng electron and the exchange-

TABLE IV. $J = 4$ MQDT parameters.

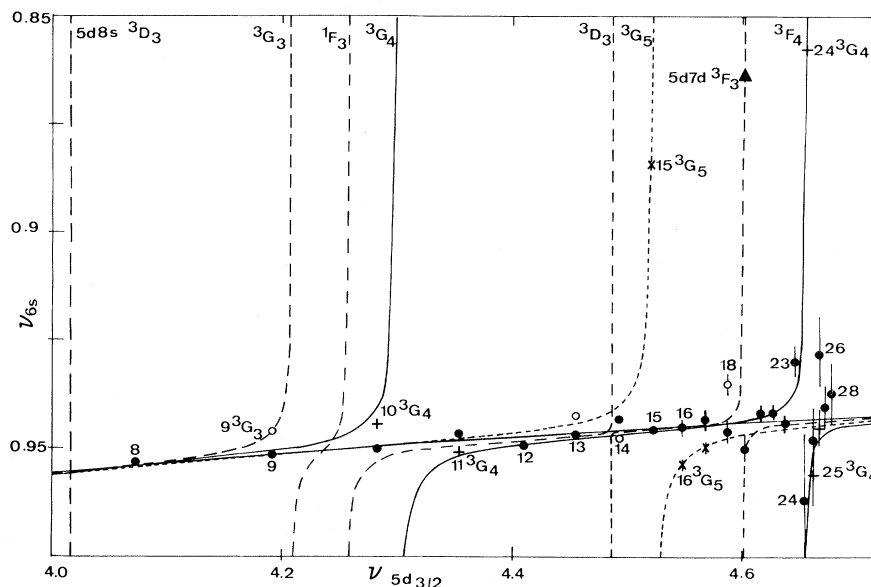| $\bar{a}, \alpha, i$	1	2	3	4	5
$\bar{a}$	$6sg$ $^3G_4$	$6sg$ $^1G_4$	$5dd$ $^3G_4$	$5dd$ $^3F_4$	$5dd$ $^1G_4$
i	$6s_{1/2}g_{7/2}$	$6s_{1/2}g_{9/2}$	$5d_{3/2}d_{5/2}$	$5d_{5/2}d_{3/2}$	$5d_{5/2}d_{5/2}$
μ_α^0	0.0585	0.0585	0.7647	0.6509	0.5372
μ_α^1	−0.8	−0.8	1.1	0.47	0.85
$U_{i\alpha}$	0.744	0.667	−0.045	0	0
	−0.665	0.745	0.040	0	0
	0.042	0	0.706	−0.316	0.632
	0.042	0	0.706	0.316	−0.632
	0	0	0	0.894	0.447

FIG. 4. Lu-Fano plot of the $6sng$ perturbed Rydberg series. Curves calculated from MQDT models compiled in the tables are — — —, $J=3$; ———, $J=4$; and ---, $J=5$. Experimental points are ●, unresolved $6sng$ $^{1,3}G$; ○, $6sng$ $^{3}G_3$; +, $6sng$ $^{3}G_4$; ×, $6sng$ $^{3}G_5$; and ▲, perturber. Perturbers located out of the figure are noted by the vertical branches they cause in the plot; $5d\,7d$ perturbers are represented by $^{2S+1}L_J$.

electrostatic interaction between the $6s$ electron and an ng electron, the fine structure of the four $6sng$ $^{3}G_{3,4,5}$ and $^{1}G_4$ is only partially resolved. Some $6sng\,^{3}G_J$ levels are identified near the $5d\,7d$ perturbers; the $6sng$ $^{3}G_3$ are observed for $n=9$, 13, 14, and 18, respectively, in the vicinity of $5d\,7d$ $^{3}G_3$, $^{3}D_3$, and $^{3}F_3$ levels; the $6sng$ $^{3}G_4$ levels are observed for $n=10$ and 11 near the $5d\,7d$ $^{3}G_4$ level and for $24 \leq n \leq 26$ near the $5d\,7d$ $^{3}F_4$ level; the $6sng$ $^{3}G_5$ levels are detected for $15 \leq n \leq 17$ near the $5d\,7d$ $^{3}G_5$ perturber.

The interpretation of the perturbed $6sng$ series is obtained with three MQDT analyses: the previous $J=3$ model (Sec. III) is extended by adding a seventh channel, the $6sng$ channel; the $J=4$ spectrum is analyzed with a five-channel model; and the $J=5$ spectrum with a two-channel model. The labeling of channels and the optimal sets of parameters are compiled in Tables II, IV, and V. Only one value of eigenquantum defect μ_G was optimized for the four $6sng$ channels from selected unperturbed levels. The high-lying $6sng$ levels ($n > 25$) affected by large experimental uncertainties are ignored. The strength of the interactions between $6sng$ and $5dnd$ channels were determined from the $6sng\,^{3}G_J$ perturbed levels; for each J value the interactions were parametrized in terms of only one angle θ_J; these angles allow one to generate the $V_{\bar{a}\alpha}$ matrix defined in Eq. (3) by coupling the $6sng\,^{3}G$ and $5dnd\,^{3}G$ channels. Notice that the three optimal angles

$\theta_3 = 0.05$, $\theta_4 = 0.06$, and $\theta_5 = 0.05$ are nearly equal. The eigenquantum defect of the perturbing $5dnd$ channels are determined from the $5d\,7d$ levels observed in CD (3) and from the lower $5d\,6d$ levels compiled by Moore.[16]

Parts of the three Lu-Fano curves obtained for the $J=3$, 4, and 5 spectra are plotted in Fig. 4. Since the lowest $6sng$ levels for $n \leq 7$ are unknown, we have only drawn the curves for $\nu_{5d_{3/2}} \geq 4.0$. Experimental points with error bars are reported for $n \leq 28$ with the labels given in CD.[14] Note that the $5d\,7d$ $^{1}G_4$ level does not appear since it is located above the $6s$ limit.

Our MQDT models predict that the $6sng$ $^{1}G_4$ series are unperturbed and that the three $6sng\,^{3}G$ series are perturbed. Although deviations between theoretical and experimental levels are often larger than the experimental uncertainty, the behavior of the perturbed $6sng\,^{3}G$ series is rather well described.

TABLE V. $J=5$ MQDT parameters.

$\bar{a},\alpha,i$	1	2
$\bar{a}$	$6sg\,^{3}G_5$	$5dd\,^{3}G_5$
i	$6s_{1/2}g_{9/2}$	$5d_{5/2}d_{5/2}$
μ_α^0	0.0585	0.7758
μ_α^1	-0.80	1.02
$U_{i\alpha}$	0.999	-0.050
	0.050	0.999

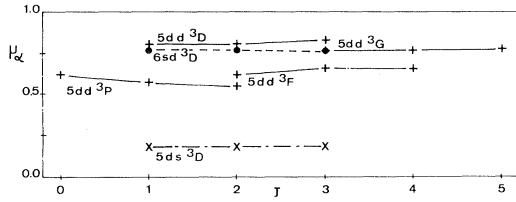FIG. 5. Variation of the eigenquantum defect μ_α^0 for a given triplet as a function of J. Symbols are ●— — —, $6sd$; + ——, $5dd$; and × —·—·; $5ds$ channels.

The perturbations due to $5d\,7d$ $^3G_{3,4,5}$ and $^3F_4$ levels are successfully reproduced in spite of the simplicity of the involved MQDT models. The largest discrepancies appear for the $J = 3$ spectrum: The two points corresponding to the perturbed $6s\,13g$ $^3G_3$ and $6s\,18g$ $^3G_3$ levels show significant differences. It should be pointed out that these levels were identified in CD[14] from the observation for each of only one line starting, respectively, from the $5d\,6d$ $^3P_2$ and $5d\,6d$ $^3D_3$ levels. Thus it appears unreasonable to try to improve our MQDT models for taking care of them. Further measurements with a higher resolution and also a better J determination are needed for improving the fit.

VI. DISCUSSION ON MQDT PARAMETERS

The values of the various μ_α^0 eigenquantum defects optimized for triplet channels in the MQDT analyses of the $J = 0-5$ spectrum, obtained either in this paper or in AC[3] and AR,[4] are plotted in Fig. 5 against the J value. For a given LS term μ_α^0 is nearly independent of the J value. In fact, the eigenquantum defect differences can be interpreted in terms of short-range interactions; the Coulomb interaction largely dominates the spin-orbit coupling so that the character of the LS coupled eigenchannel α is essentially the same for different J values. This property of eigenquantum defect was already emphasized in Refs. 8 and 18.

All the eigenquantum defects μ_α determined for the $6snl$ or $5dnd$ series decrease with increasing energy which means that the μ_α^1 are positive with the convention defined in Eq. (2). This downward drift follows the normal trend of scattering phase shifts due to an attractive potential. However, the optimized μ_α^1 values are only approximate. In fact, the μ_α value corresponding to a given $5dnl$ channel is determined from only two levels. Moreover, it has been shown[11] that an imprecise determination of interaction parameters, due in particular to the neglect of the energy dependence of these parameters, can lead to the determination of incorrect μ_α^1 values. In

our work the interaction angles are mainly determined only from the high-lying perturbed levels. The choice we have made for the interaction angles is not unique, and further measurements are very worthwhile in the intermediate energy range to check or improve the fit.

Recently, various alkaline-earth MQDT parameters have been determined by *ab initio* calculations performed by Armstrong *et al.*[19] who used a local approximation for the exchange-correlation potential seen by the Rydberg electron. The quantum-defect parameters of $6sns$ ^3S and $6snd$ ^3D channels, calculated by neglecting interchannel interaction and spin-orbit coupling, are compared with our empirical values in Table VI. Our μ_α^0 values are smaller than *ab initio* values, while the μ_α^1 values are in good agreement taking into account the dispersion of our $\mu^1_{3_{D_J}}$ values.

VII. CONCLUSION

The MQDT models presented in this paper in addition to those previously developed in AC[3] and AR[4] provide an accurate description of the even-parity bound spectrum of Ba. This MQDT treatment is by far the most complete of those carried out for a bound spectra of alkaline-earth atoms since almost all bound levels with J values ranging from 0 to 5 have been considered. A unified treatment of new data provided by laser spectroscopy[3,15] and earlier data of Moore[16] has been developed.

The behavior of all $6snl$ series ($l = s,d,g$) perturbed by many levels pertaining to doubly excited configurations is successfully interpreted. Although MQDT performs a J by J treatment of a given-parity spectrum, is permits us to obtain a good description of anomalous fine structure of highly excited $6snd$ and $6sng$ configurations. Additional experimental data are required to improve the MQDT analyses for some intermediate $6snd$ $^3D_1$ and $6sns$ $^3S_1$ levels and also for $6sng$ levels, the fine structure of which is only partially resolved.

The MQDT parametrization of energy levels pro-

TABLE VI. Comparison of empirical eigenquantum defects [this work and AR (Ref. 4)] with *ab initio* values (Ref. 19) calculated by ignoring spin-orbit coupling.

Channel	Eigenquantum defect	
	Empirical values	*a priori* values
$6ss$ $^3S_1$	$0.29 + 0.3\epsilon$	$0.24 + 0.38\epsilon$
$6sd$ $^3D_1$	$0.7715 + 1.0\epsilon$ ⎱	
$6sd$ $^3D_2$	$0.7668 + 1.03\epsilon$ ⎰	$0.89 + 0.64\epsilon$
$6sd$ $^3D_3$	$0.760 + 0.66\epsilon$	

vides information not only on energy determination but also on wave functions. Our study confirms the previous designations of levels. As already pointed out in CD[13] the jj coupling scheme is better suited to describe the $5dnd$ levels than the LS coupling scheme. The accuracy of the wave functions can be checked when experimental data on atomic quantities are available: Very recently,[20−22] lifetime measurements performed for $6snd\,^{1,3}D_2$ and $6sns\,^1S_0$ perturbed levels provided a good probe of MQDT

functions previously published in AC[3] and AR.[4]

For the first time the J dependence of MQDT parameters in Ba is analyzed; this allows us to predict the ζ_{nd} spin-orbit parameter of the highly excited nd electrons.

ACKNOWLEDGMENT

[1]D. J. Bradley, P. Ewart, J. V. Nicholas, and J. R. D. Shaw, J. Phys. B **6**, 1594 (1973).

[2]J. R. Rubbmark, S. A. Borgström, and K. Bockasten, J. Phys. B **10**, 412 (1977).

[3]M. Aymar, P. Camus, M. Dieulin, and C. Morillon, Phys. Rev. A **18**, 2173 (1978).

[4]M. Aymar and O. Robaux, J. Phys. B **12**, 531 (1979).

[5]J. J. Wynne and J. A. Armstrong, IBM J. Res. Dev. **23**, 490 (1979).

[6]M. J. Seaton, Proc. Phys. Soc. London **88**, 801 (1966).

[7]K. T. Lu and U. Fano, Phys. Rev. A **2**, 81 (1970).

[8]K. T. Lu, Phys. Rev. A **4**, 579 (1971).

[9]C. M. Lee and K. T. Lu, Phys. Rev. A **8**, 1241 (1973).

[10]U. Fano, J. Opt. Soc. Am. **65**, 979 (1975).

[11]J. A. Armstrong, J. J. Wynne, and P. Esherick, J. Opt. Soc. Am. **69**, 211 (1979).

[12]J. J. Wynne and J. P. Hermann, Opt. Lett. **4**, 106 (1979).

[13]P. Camus, M. Dieulin, and C. Morillon, J. Phys. (Paris) **40**, L513 (1979).

[14]P. Camus, M. Dieulin, and A. El. Himdy, Phys. Rev. A **26**, 379 (1982).

[15]O. Robaux and M. Aymar, Comput. Phys. Commun. **25**, 223 (1982).

[16]C. E. Moore, *Atomic Energy Levels*, Natl. Bur. Stand. (U.S.) NO. 467, Vol. 3 (U.S. GPO, Washington, D.C., 1958).

[17]E. U. Condon and G. H. Shortley, *The Theory of Atomic Spectra* (Cambridge University Press, Cambridge, England, 1963).

[18]M. Aymar, O. Robaux, and C. Thomas, J. Phys. B **14**, 4255 (1981).

[19]J. A. Armstrong, Sudhanshu S. Jha, and K. C. Pandey, Phys. Rev. A **23**, 2761 (1981).

[20]T. F. Gallagher, W. Sandner, and K. A. Safinya, Phys. Rev. A **23**, 2669 (1981).

[21]M. Aymar, R. J. Champeau, C. Delsart, and J. C. Keller, J. Phys. B **14**, 4489 (1981).

[22]M. Aymar, P. Grafström, C. Levinson, H. Lundberg, and S. Svanberg, J. Phys. B **15**, 877 (1982).